Journal Website: https://www.icjn.net/jswvcm ISSN: 3106-5139 | EISSN: 3106-5147

Journal of Solid Waste Valorization and Chemical Management (JSWVCM)

ICJN Press Volume. 01 | Issue. 02 | Aug. 2026 DOI: 10.66729/jswvcm202604201

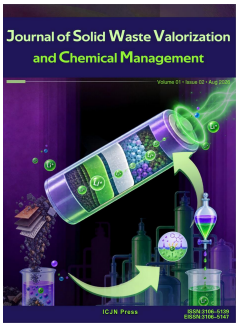

REVIEW

A Review of DFT Studies in Biomass Pyrolysis and Gasification

Ying Wang[1], Baofeng Zhao[1,*], Chongmin Wang[1], Haibin Guan[1], Lei Chen[1], Bari Wulan[1], Laizhi Sun[1], Tianyi Liu[1], Krishnaswamy Nandakumar[1], Wanning Zheng[2], Ying Bo[3]

1 Energy Research Institute, Shandong Key Laboratory of Biomass Efficient Conversion and Utilization, Qilu University of Technology (Shandong Academy of Sciences), Jinan Shandong 250014, China.
2 Jinan Shanyuan Environmental Protection Technology Co., Ltd, Jinan Shandong 250013, China.
3 Shandong Yimeike Energy Conservation Service Co., Ltd., Jinan Shandong 250000, China.

*Corresponding Author: Baofeng Zhao, E-mail: zhaobf@sderi.cn

Abstract

Biomass thermochemical conversion is a key route for converting renewable carbon into fuels and high-value chemicals, and density functional theory (DFT) has been used to elucidate its microscopic mechanisms. This review summarizes DFT studies of reaction pathways, key intermediates, and catalyst-surface mechanisms in four core fields of biomass pyrolysis and gasification. In biomass primary pyrolysis, main model compounds of cellulose, hemicellulose and lignin, such as cellobiose, xylan fragments and lignin β-O-4 dimers, have been used to analyze glycosidic-bond, Cβ–O and Cα–Cβ cleavage, hydrogen transfer, dehydration and transglycosylation pathways leading to levoglucosan, 5-hydroxymethylfurfural, furfural and phenolic products. For bio-oil upgrading, DFT calculations on Pt, Fe, Ru–H_2O, Mo_2C and Co@CoO systems have revealed the effects of adsorption geometry, hydrogen activation and transfer, and C–O cleavage on hydrogenation, dehydroxylation and demethoxylation routes and product selectivity. For tar removal, DFT studies have calculated initial C–H/O–H cleavage, aromatic-ring opening and carbon-removal steps of toluene and phenol on transition-metal, CaO-based and carbon-based catalysts, and analyzed the effects of surface composition and interfacial structure on cracking and reforming. In gas conditioning, DFT studies have attempted to describe competitive and synergistic radical reactions of surface carbon, CH_x, O, OH, and H intermediates linking methane reforming, carbon removal, and water-gas shift/reverse water-gas shift reactions (WGS/RWGS). In conclusion, the molecular mechanism of biomass thermal conversion could be elucidated and consistent with macroscale reaction tendencies via DFT simulations; nevertheless, the relatively simplified compound models of biomass and catalytic surface models, isolated elementary steps and limited kinetic descriptions led to considerable discrepancies between computational results that still fail to perfectly reproduce authentic reaction behaviors. Future work should integrate realistic catalytic structures, interconnected reaction networks, microkinetic modelling, and experimental validation to more accurately design chemical reactions and forecast product distributions for engineering applications of solid waste utilization.

Keywords

Biomass thermochemical conversion; DFT; Primary pyrolysis; Tar removal; Bio-oil upgrading; Syngas conditioning

Citation: Ying Wang, Baofeng Zhao, Chongmin Wang, *et al*. A Review of DFT Studies in Biomass Pyrolysis and Gasification. *Journal of Solid Waste Valorization and Chemical Management*. 2026, 01 (2): 1-16. doi: 10.66729/jswvcm202604201.

Copyright:© 2026 The Author(s). Published by ICJN Press.
This is an open access article under the https://creativecommons.org/licenses/by/4.0/
Received 20 April 2026; Revised 7 July 2026; Accepted 7 August 2026; Available online 27 August 2026.

Graphical Abstract

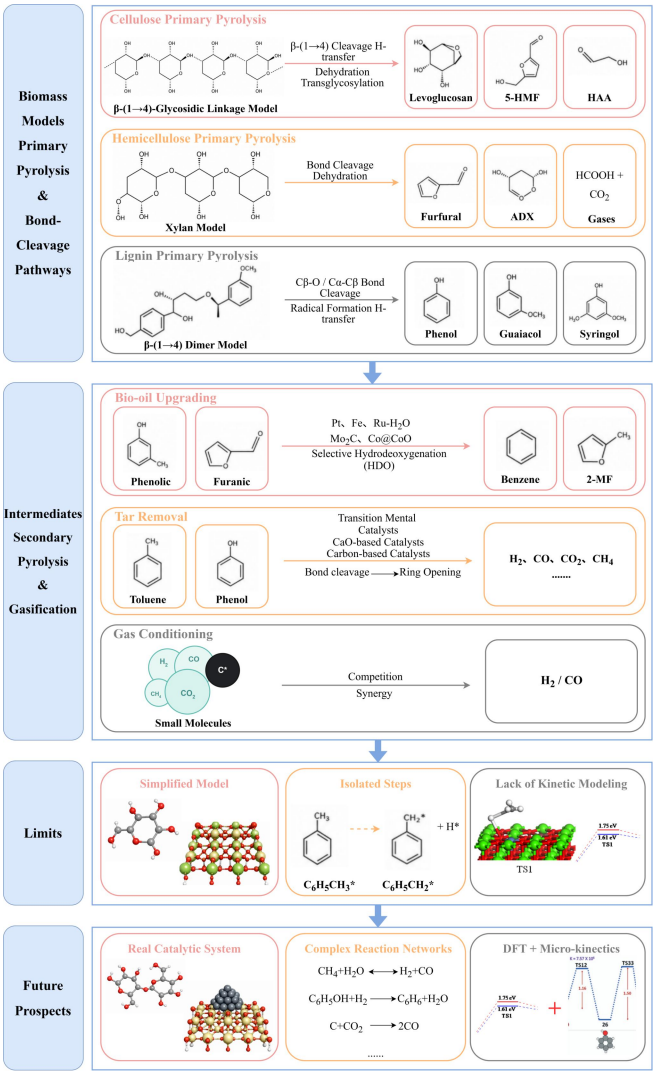

NOTE: 5-HMF: 5-hydroxymethylfurfural; HAA: hydroxyacetaldehyde; ADX: 1,4-anhydro-D-xylopyranose; HDO: hydrodeoxygenation; 2-MF: 2-methylfuran; DFT: density functional theory; TS: transition state; C^* and H^* represent adsorbed carbon and adsorbed atomic hydrogen, respectively; $C_6H_5CH_3^*$and $C_6H_5CH_2^*$ represent adsorbed toluene and benzyl species, respectively. Copyright: Created by the authors using draw.io (diagrams.net, web version 30.3.13), a freely available, open-source diagramming tool.

Highlights

- Applications of DFT in biomass thermochemical conversion were systematically reviewed.
- DFT could elucidate the molecular mechanisms underlying catalytic biomass thermochemical conversion.
- Coupling DFT with kinetic modeling and ML could enable realistic predictions of biomass conversion behavior under engineering-relevant conditions.

1. Introduction

Biomass solid waste broadly includes agricultural and forestry residues, food-processing residues, and food and kitchen waste. Lignocellulosic residues are widely distributed, compositionally heterogeneous renewable carbon resources. If improperly managed, their accumulation, open burning, or uncontrolled disposal may generate odours, leachate, and particulate emissions, resulting in environmental pollution and the loss of recoverable carbon resources. Thermochemical conversion can transform these residues into bio-oil, syngas, biochar, fuels, and chemical intermediates. density functional theory (DFT) simulations can provide molecular-level mechanistic insight into biomass thermochemical conversion and generate parameters that support process optimization at the engineering scale, thereby facilitating industrial deployment, reducing environmental pollution, and promoting the clean valorization of waste biomass. The resulting oxygenates, aromatic fragments, light gases, and solid carbon undergo secondary cracking, deoxygenation, reforming, and condensation, linking primary pyrolysis with tar formation, bio-oil evolution, and syngas conditioning[1-6]. These

coupled reactions strongly influence carbon efficiency, product quality, tar and coke formation, and the environmental performance of the thermochemical valorization of waste biomass.

Pyrolysis gas chromatography/mass spectrometry (Py-GC/MS) and thermogravimetric analysis coupled with Fourier transform infrared spectroscopy (TG-FTIR) characterize product evolution, whereas in situ spectroscopy can probe adsorbed surface species. These techniques, however, seldom resolve short-lived intermediates or discriminate among competing elementary pathways. DFT complements this evidence by comparing candidate pathways, locating intermediates and transition states, and relating activation energetics to interfacial electronic structure[7-9]. DFT evidence in this field should therefore be read as a model-conditioned mechanistic argument rather than as a direct predictor of industrial conversion performance. Calculated adsorption energies and activation barriers depend not only on the selected molecule or surface, but also on the exchange-correlation functional, dispersion treatment, spin and charge description, and transition-state verification. Dispersion corrections are particularly relevant for aromatic tars, phenolics and furanic oxygenates, because π–surface and van der Waals interactions can change adsorption geometry and consequently alter the apparent first activation step. For transition states, locating a saddle point is not sufficient by itself; the structure should be connected to the intended reactant and product states through frequency analysis and, where possible, intrinsic reaction-coordinate checks. In high-temperature pyrolysis, reforming and (water-gas shift/reverse water-gas shift reactions) WGS/RWGS environments, 0 K electronic energies also cannot be equated directly with working barriers, because entropy, surface coverage and gas-phase chemical potentials may change the relative importance of parallel pathways. These uncertainties become more pronounced for reducible oxides, magnetic systems and metal-support interfaces. Ni-, Fe-, CeO_2- and Fe_2O_3-based catalysts may involve multiple spin states, oxygen vacancies, oxidation states and interfacial charge distributions; therefore, DFT+U choices, slab termination and vacancy models can influence calculated C–H activation, O/OH transfer, carbon removal and WGS/RWGS energetics. Small differences in activation barriers, especially differences of only a few tenths of an electronvolt, should therefore not be overinterpreted as a universal activity order unless they are supported by consistent computational protocols, sensitivity checks or discriminating experiments. A more reliable use of DFT is to identify plausible elementary steps, descriptors and competing pathways, and then constrain these interpretations with Py-GC/MS, in situ diffuse reflectance infrared Fourier transform spectroscopy (DRIFTS), temperature-programmed desorption (TPD) cannot fully capture, isotope tracing, in situ/operando spectroscopy and kinetic or microkinetic analysis. Experimental evidence is treated here as a constraint on DFT interpretation, not as a simple confirmation of a calculated pathway. Product distributions from Py-GC/MS or TG-FTIR can show whether a proposed route is chemically plausible, but they rarely identify a unique transition state. Surface-sensitive methods such as DRIFTS, TPD, ambient-pressure X-ray photoelectron spectroscopy (AP-XPS), isotope tracing and operando spectroscopy can narrow the range of possible adsorbed intermediates and working sites, although they still depend on time scale, detection window and reaction environment. From an environmental-engineering perspective, these DFT-derived pathways and energetics can be used to identify the molecular steps governing tar and coke formation, carbon retention, oxygen removal and H_2/CO regulation, thereby providing mechanistic constraints for pollution control and the clean resource utilization of waste biomass.

Existing reviews have examined complementary but largely separate parts of biomass thermochemical conversion. Bridgwater focused on fast-pyrolysis technologies[4], bio-oil properties and upgrading routes, whereas Zhang and Huang reviewed DFT and reactive force field molecular dynamics (ReaxFF MD) studies of lignin pyrolysis[10], including bond cleavage, reaction pathways and char formation. Taken together, these reviews do not connect DFT-derived mechanisms of cellulose, hemicellulose and lignin pyrolysis with downstream tar removal, bio-oil upgrading and syngas conditioning. The present review follows this linked conversion sequence to distinguish robust mechanistic trends from conclusions that depend on simplified models. It also identifies which mechanistic interpretations are supported by experiments and which remain difficult to relate to process behavior.

This review examines DFT studies in four interconnected process domains of biomass thermochemical conversion: primary pyrolysis, tar removal, bio-oil upgrading, and syngas conditioning. **Figure. 1** outlines this process-based organization and the four cross-cutting analytical dimensions applied throughout: mechanistic synthesis, model and methodological validity, experimental corroboration, and engineering relevance. Sections 2–5 examine these domains, while Section 6 synthesizes their shared methodological limitations and research priorities. Across these sections, robust mechanistic trends are distinguished from model-dependent interpretations, and their implications for catalyst and process design in waste biomass valorization are critically assessed.

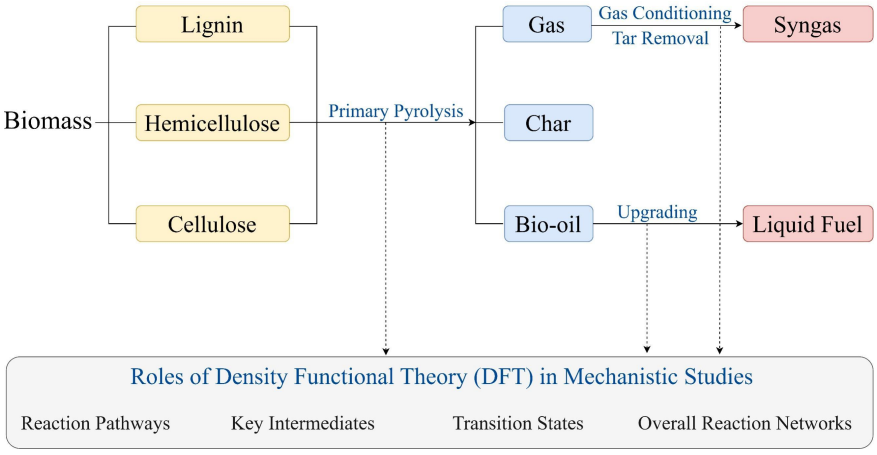

Figure.1 Schematic of biomass conversion and DFT modeling focus. Copyright: The figure was created by the authors using draw.io (diagrams.net, web version 30.3.13).

2. DFT Research on Primary Pyrolysis of Biomass

Primary biomass pyrolysis is mainly investigated through its three major constituents: cellulose, hemicellulose, and lignin. Owing to the structural complexity of natural biomass, heterogeneous local environments, and multiple parallel reactions, direct quantum-chemical calculations on intact macromolecules are generally infeasible. Accordingly, DFT studies usually adopt representative monomeric or dimeric models, including glucose and cellobiose for cellulose, xylose, xylobiose, and branched xylan fragments for hemicellulose, and β-O-4 dimers for lignin. These simplified models do not provide the same level of structural information and therefore cannot be used to address the same mechanistic questions. Even when a DFT calculation is numerically converged, its applicability depends on whether the selected model contains the structural feature involved in the reaction. Glucose can be used to investigate dehydration and ring opening, whereas cellobiose is needed to examine cleavage of the β-(1→4)-glycosidic linkage. Similar considerations apply to branched xylan fragments and β-O-4 lignin dimers. **Table 1** summarizes the structural features retained by these commonly used models and the reactions they can be used to examine.

Table 1. Applicability and structural limitations of molecular models used in DFT studies of primary biomass pyrolysis

Biomass Fraction	Model Used in DFT	Structural Feature Retained	Mechanistic Role
Cellulose	Glucose[11,12]	Glucopyranose ring and hydroxyl groups	Local dehydration, ring opening, H-transfer and furan formation
	Cellobiose[7,11,13]	One β-(1→4)-glycosidic linkage between two glucosyl residues	Glycosidic-bond cleavage, concerted transglycosylation, and competition among levoglucosan (LG), hydroxyacetaldehyde (HAA), and 5-HMF-forming pathways
Hemicellulose	Xylose[14]	Xylopyranose ring and hydroxyl groups	Pentose ring opening, dehydration and furfural formation
	Xylobiose[14]	One β-(1→4)-xylosidic linkage between two xylosyl residues	Xylosidic-bond cleavage and product formation
	Branched xylan fragments[15,16]	A selected xylan backbone segment containing an explicit side group	Side-group cleavage and acid/CO_2 formation
Lignin	β-O-4 dimer[8,17,18]	One aryl ether linkage with an adjacent side chain and selected aromatic substituents	β-O-4 cleavage, side-chain scission and phenolic-product formation

NOTE: 5-HMF: 5-hydroxymethylfurfural.

Idealized small-molecule models that retain selected structural features can reproduce trends consistent with those of real macromolecular biomass; however, their representativeness remains limited. For example, glucose can be used to investigate dehydration, ring opening, and hydrogen transfer within a monosaccharide unit, but it cannot describe cleavage of the β-(1→4)-glycosidic linkage. Cellobiose retains one glycosidic linkage but does not reproduce the degree of polymerization, crystalline structure, or long-range hydrogen-bonding network of native cellulose. Branched xylan fragments can represent selected side chains but cannot capture the complex substitution patterns and branch distributions of native xylan. A β-O-4 dimer can be used to examine Cβ-O and Cα-Cβ bond cleavage, but it cannot fully represent the diversity of lignin interunit linkages or radical repolymerization.

2.1 Cellulose

Cellulose is a linear polymer of β-D-glucose units linked by β-1,4-glycosidic bonds. Because native cellulose is too large for direct DFT treatment, studies generally adopt simplified monosaccharide and disaccharide models.

Monosaccharide models are used mainly to examine dehydration, ring opening and intramolecular rearrangement within glucose units. They are useful for explaining products such as levoglucosan (LG), 5-hydroxymethylfurfural (5-HMF) and their degradation products. Wang *et al*. combined Py-GC/MS with DFT to investigate the pyrolysis of cellulose-derived model compounds, including cellobiose and glucose[11], and showed that the major products mainly include pyrans, furans, and light linear oxygenates. DFT was mainly used to compare plausible formation pathways of characteristic products on the basis of a D-glucopyranose unit. The results suggested that glucose- and cellobiose-derived products exhibit a stronger tendency toward furan formation. Along the same line, Hu *et al*. further employed glucose and mannose as monosaccharide models to investigate the formation of 5-HMF and furfural[12]. In these studies, DFT helps distinguish intermediates, transition states and barriers among dehydration and rearrangement routes. However, monosaccharide models cannot directly describe cleavage of the β-1,4-glycosidic linkage.

By contrast, disaccharide models explicitly retain the β-1,4-glycosidic bond and are therefore better suited to probing initial chain scission of the cellulose backbone and the competition among major product-formation pathways. Zhang *et al*. pointed out that glucose cannot adequately describe cellulose backbone cleavage because it lacks the β-1,4-glycosidic linkage[13]. They therefore selected cellobiose as the model compound and proposed an initial pyrolysis network containing ten pathways. Their results showed that H-assisted activation of the glycosidic bond promotes cleavage of the C1′-O4 bond, whereas concerted transglycosylation is another key route for generating LG-related intermediates; overall, glycosidic-bond cleavage (Pathway 1) and concerted transglycosylation (Pathway 8) constitute two competing parallel pathways. Wang *et al*. further combined experiments and theory to compare the product distributions of cellulose and cellobiose under different temperature gradients[7], showing that both systems generate the same major products, including LG, HAA, 5-HMF, and furfural, and that the corresponding reaction network can be grouped into four channels: LG formation, HAA formation, 5-HMF formation, and dehydration.

Thus, DFT studies of cellulose have moved from monosaccharide units to disaccharide models that retain the glycosidic bond. Glucose is mainly used to examine reactions within a single sugar unit, such as dehydration, ring opening and furan formation. Cellobiose contains the β-(1→4)-glycosidic linkage and can therefore be used to study initial chain cleavage and transglycosylation. Py-GC/MS results show that cellulose and cellobiose produce similar major products, although their relative yields are different[7,11]. This agreement supports the proposed formation pathways of the main products, but it does not prove that only one reaction pathway or transition state is involved. In addition, cellobiose does not reproduce the degree of polymerization or crystalline hydrogen-bonding network of cellulose. Therefore, the calculated pathways and barriers should be understood as results obtained from the selected model rather than as direct predictions of cellulose product yields.

2.2 Hemicellulose

Xylan typically features a xylan backbone, whilst also containing side groups such as O-acetyl and 4-O-methylglucuronosyl. As the xylan backbone is relatively short and rich in side chains, primary pyrolysis studies of xylan must not only consider the reactions of the xylan backbone itself, but also account for the effects of glycosidic bonds and side-chain structures. Previous DFT studies typically use xylose and xylobiose as model molecules, and subsequently extend to xylan model molecules with complete branching structures.

Using xylobiose as the model compound, DFT mainly clarifies the role of the β-1,4-glycosidic bond in main-chain pyrolysis. Hu *et al*. reported that the overall reaction mechanism of xylobiose is similar to that of xylose[14], but that the presence of the glycosidic bond changes the formation efficiency of key intermediates and thus shifts product distribution. At 400 °C, the major products of xylobiose pyrolysis still include hydroxyacetaldehyde (HAA), furfural, di-dehydrated xylose (DAX), and 1,4-anhydro-D-xylopyranose (ADX), with ADX remaining one of the dominant products; compared with xylose, however, xylobiose yields a higher fraction of dehydrated sugars such as DAX. Thus, the xylobiose model does not alter the basic reaction framework established for xylose pyrolysis, but instead incorporates the effect of the glycosidic bond and thereby explains variations in the distribution of intermediates and major products.

When the scope of study is extended from xylobiose to more realistic xylan structures, side chains become a key factor governing the initial pyrolysis behavior. In this context, xylose, xylobiose, and xylan-based structures have been widely adopted as representative model compounds in mechanistic studies of hemicellulose pyrolysis[19]. A representative example is the work of Hu *et al*. who combined experiments and DFT calculations to compare the pyrolysis behavior of xylose, xylobiose, and xylan model compounds[14]. More recently, Hu *et al*. further compared the effects of different branch types[15]. Combining xylans from different sources with TG-FTIR, Py-GC/MS, and DFT calculations, they showed that branch units, especially uronic acid groups, preferentially decompose during the initial stage, releasing formic acid and CO_2. Arabinose side chains tend to undergo C-O cleavage on the side-chain side, whereas uronic acid units more readily cleave the C-O bond linking the branch to the main chain. Different side-chain types therefore reshape the pool of initial intermediates and ultimately alter product distribution.

The studies discussed above show that side groups are important in hemicellulose pyrolysis. Xylose can be used to examine ring opening, dehydration, and furfural formation, while xylobiose also contains the β-(1→4)-xylosidic linkage needed to study backbone cleavage. However, neither model includes the acetyl, arabinosyl or uronic-acid groups present in many natural xylans. Experiments on branched xylans show that these groups affect the early release of organic acids and CO_2 and alter the distribution of subsequent products[14-16]. The corresponding DFT models help explain how particular side groups are cleaved, but each model represents only one selected branch structure. TG-FTIR and Py-GC/MS provide evidence from gas evolution and product distributions, although they cannot by themselves identify all intermediates or determine a unique microscopic pathway. The results obtained from one branched fragment therefore cannot be applied directly to hemicelluloses with different branch compositions and substitution patterns.

2.3 Lignin

Lignin is a structurally heterogeneous aromatic polymer derived mainly from three phenylpropanoid units: p-hydroxyphenyl (H), guaiacyl (G), and syringyl (S)[20]. These units are connected through multiple interunit linkages, including β-O-4, α-O-4, 4-O-5, β-1, and 5-5 bonds. Among them, β-O-4 is generally the most abundant aryl ether linkage and has therefore become the most widely used structural motif in DFT studies of lignin pyrolysis. β-O-4 dimer models are particularly useful for evaluating Cβ-O and Cα-Cβ bond dissociation, radical cleavage, concerted decomposition pathways, and the formation of primary phenolic monomers. However, such simplified dimer models cannot fully capture the structural heterogeneity, condensed linkages, substituent effects, and secondary repolymerization behavior of real lignin-derived intermediates.

Huang *et al*. used 1-phenyl-2-phenoxy-1,3-propanediol as an unsubstituted β-O-4 dimer model and calculated the bond dissociation energy (BDE) of its major bonds using DFT[17]. The Cβ-O bond showed the lowest BDE (245.3 kJ/mol), followed by the Cα-Cβ bond (259.2 kJ/mol), indicating that Cβ-O homolysis is the most favorable initial scission pathway, with Cα-Cβ homolysis as a competing route. Shen *et al*. further employed a more substituted guaiacol-based β-O-4 dimer and investigated its pyrolysis by combining Py-GC/MS with DFT calculations[8]. Their experiments identified 2-methoxy-4-vinylphenol and 2-methoxyphenol as the major products, while the DFT calculations indicated that Cβ-O homolysis was the key initial step leading to both compounds. The former was mainly formed through hydrogenation followed by dehydration, whereas the latter resulted mainly from hydrogenation. Elder and Beste further showed, based on β-O-4 model compounds[18], that concerted cleavage pathways should also be considered in addition to radical homolysis, with retro-ene cleavage exhibiting kinetic advantages.

The fate of the primary products becomes more complex after the initial β-O-4 cleavage. Bai *et al*. combined online Py-GC/MS with gel permeation chromatography (GPC) and atmospheric-pressure photoionization high-resolution mass spectrometry to characterize lignin-derived products[21]. Their results showed that reactive products such as guaiacol, syringol, and 2-methoxy-4-vinylphenol can form phenolic dimers and oligomers during fast pyrolysis. Hosoya *et al*. further found that lignin-derived primary tar can undergo condensation and side-chain cracking in parallel[22]. These studies indicate that lignin-derived intermediates do not follow a single secondary reaction route.

Depending on the reaction conditions, some lignin-derived

intermediates remain as volatile phenolics, whereas others form condensable phenolic oligomers or contribute to the solid carbonaceous residue. DFT calculations using an S-type β-O-4 dimer have also suggested competition between gas-forming reactions and a cyclization route leading to char precursors[23]. However, this calculation describes one dimer model and one possible char-forming route. It does not reproduce the diversity of lignin linkages, intermolecular radical reactions, or the effects of residence time and phase behaviour. Heavy tar and phenolic oligomers may subsequently contribute to coke formation during catalytic tar removal or bio-oil upgrading. Coke formation is therefore more appropriately associated with the downstream catalytic conversion of these products than with primary lignin pyrolysis itself.

These studies show that β-O-4 dimer models provide useful information on initial bond cleavage and the formation of primary phenolic products, but much less information on secondary repolymerization. Py-GC/MS identifies the main volatile products, whereas GPC and high-resolution mass spectrometry provide information on heavier oligomers[8,21]. Even when these experiments are combined with DFT, the relative contributions of volatilization, repolymerization, and solid-carbon formation remain difficult to determine.

2.4 Comparison of Model Representativeness in DFT Studies of Primary Biomass Pyrolysis

The studies discussed in Sections 2.1–2.3 use models with different levels of structural detail. Glucose and xylose are mainly used to examine reactions within a single sugar unit, whereas cellobiose and xylobiose retain one β-(1→4)-glycosidic linkage and can therefore be used to study initial chain cleavage. Branched xylan fragments include selected side groups, while β-O-4 dimers retain one common linkage in lignin. These models make it possible to examine reactions that cannot be described using monomers alone, but they do not reproduce the complete polymer structure. For example, the sugar models omit crystallinity and long-range hydrogen bonding, whereas short lignin dimers omit linkage diversity and intermolecular radical reactions. The conclusions obtained from each model should therefore remain linked to the structural feature included in that model.

Several reactions appear repeatedly in studies of cellulose, hemicellulose and lignin, including C-O bond cleavage, hydrogen transfer, dehydration and the formation of smaller oxygenated products. Comparison of the available studies indicates that cleavage of oxygen-containing linkages is a recurrent early event in the primary pyrolysis of cellulose-, hemicellulose-, and lignin-derived models, but it should not be regarded as a universal first step. In cellulose, cleavage of the β-(1→4)-glycosidic C-O linkage competes with concerted transglycosylation, whereas monosaccharide models can undergo dehydration, ring opening, and intramolecular rearrangement without glycosidic-bond cleavage[7,11-13]. In hemicellulose, both backbone and side-chain C-O bonds participate in the initial reaction network, but the preferred cleavage position depends strongly on the glycosidic linkage, branch type, and substitution pattern[14-16]. For β-O-4 lignin dimers, Cβ-O homolysis is often energetically favourable, while Cα-Cβ scission and concerted retro-ene fragmentation remain viable competing pathways depending on the side-chain structure and reaction conditions[8,17,18]. Therefore, the cross-component mechanistic rule is not that the three biomass fractions undergo an identical initial C-O cleavage, but that oxygen-containing structural motifs frequently define the early branching of their reaction networks, while local molecular structure determines the dominant pathway.

3. DFT Research on Tar Removal

Tar remains a major operational constraint in biomass pyrolysis and gasification because it contains condensable monocyclic and polycyclic aromatics, phenolic compounds and other oxygenated species. Condensation causes pipeline blockage and corrosion, whereas insufficient tar conversion can favour coke deposition and catalyst deactivation. Effective tar conversion consequently affects gas cleaning, carbon conversion, syngas composition and long-term process stability.

DFT studies on tar removal have mainly examined how tar compounds bind to catalyst surfaces and which elementary step initiates their decomposition. For benzene, toluene and phenol, the preferred pathway changes with both molecular structure and surface chemistry. Calculations on Ni, CaO, iron oxides and supported metals have identified different routes involving dehydrogenation, C-O or C-C bond cleavage, and aromatic-ring opening.

Most of these conclusions, however, are based on one model compound reacting on a clean, static surface. Such calculations are useful for comparing individual pathways, but they do not reproduce the competitive adsorption that occurs in a tar mixture. They also omit the effects of steam, CO_2, coke deposition and changes in catalyst structure during reaction. **Table 2** summarizes the catalyst and molecular models used in existing studies.

Table 2. Representative activation steps and catalytic performance in DFT studies of tar removal

Catalyst Type	Representative Model	Dominant Activation Step and Barrier	Experimental Performance	Reference
Transition-Metal Catalysts	Ni-based surfaces: toluene/benzene/phenol	Initial methyl C-H cleavage; 72 kJ mol^{-1} → 51 kJ mol^{-1} after B incorporation	Not reported for the representative DFT comparison	[24-26]
CaO-Based Catalysts	Toluene on Ni-Fe/CaO	H_2-forming rate-determining step; 1.50 eV→ 0.58 eV after Fe addition	98.11% conversion and 93.11% H_2 yield at 650 °C	[27,28]
Carbon-Based Catalysts	Toluene on biochar-supported Ni	Activation at low-coordination Ni sites; barrier not consistently reported	Turnover Frequency (TOF) of 1.64 s^{-1} at 600 °C; 81.60% conversion after 190 min	[29,30]
External-Field-Assisted Catalysts	Phenol on Ni/CaO-$Ca_{12}Al_{14}O_{33}$	Ring opening; 1.23 eV → 0.85 eV under 80 mT	98.70% conversion at 700 °C and 80 mT; H_2 and CO yields increased by 25.10% and 60.70%	[31]

3.1 Transition Metal Catalysts

The initial step in tar decomposition varies with both the molecule and the catalyst surface. On Ni(111), benzene first undergoes ring dehydrogenation, whereas toluene and phenol begin with methyl C-H and O-H cleavage, respectively. Benzene behaves differently on hematite. Adsorption is weak on the Fe-terminated α-Fe_2O_3(0001) surface, while the Fe/O-coexposed α–Fe_2O_3(01$\bar{1}$2) surface promotes aromatic C-C cleavage. Adsorption energy alone therefore does not describe these differences; the subsequent activation barriers must also be considered.

Calculations on Ni(111) show that toluene decomposition begins at the methyl group. Trinh *et al*. used toluene as a model compound and constructed DFT models on Ni(111) and B-doped Ni(111) to examine its activation and decomposition[25]. They showed that, on Ni(111), toluene first undergoes C-H cleavage at the methyl side chain, followed by progressive side-chain dehydrogenation; only after complete dehydrogenation do ortho C-H activation and subsequent ring opening become favorable. This suggests that the key role of Ni surfaces in tar removal is to channel aromatic molecules through side-chain dehydrogenation, thereby creating an entry point for subsequent ring activation and deep cracking. The initial pathway also varies among tar model compounds. On Ni(111), benzene first undergoes ring dehydrogenation, whereas toluene and phenol begin with methyl C-H and O-H cleavage, respectively[26]. The reported rate-limiting steps were the first ring dehydrogenation for benzene (1.57 eV), ring opening for toluene (1.67 eV), and ring dehydrogenation after O-H cleavage for phenol (1.74 eV). Because these barriers correspond to different elementary steps, they should not be interpreted as a simple activity order. In contrast, Fe-based oxide surfaces emphasize destabilization of the aromatic ring through surface-site cooperation. Huang and Cheng used benzene as a model compound to construct α-Fe_2O_3(0001) and α–Fe_2O_3(01$\bar{1}$2) surface models[24]. They found that the Fe-terminated(0001) surface is dominated by van der Waals adsorption and is largely inactive toward aromatic C-C bond cleavage, whereas the mixed Fe/O-exposed α–Fe_2O_3(01$\bar{1}$2) surface weakens ring aromaticity through strong C-O interactions and promotes aromatic C-C cleavage via the cooperative action of Fe and surface O sites, generating chain-like alkene and carbonyl intermediates. The role of Fe-based oxides in tar removal therefore lies not simply in adsorption at metal sites, but in destabilizing the aromatic skeleton through metal-oxygen synergy.

On Ni(111), the first step depends on the molecular substituent, with benzene, toluene, and phenol following different dehydrogenation routes before ring opening. On α-Fe_2O_3, aromatic C-C cleavage depends instead on the simultaneous involvement of exposed Fe and O sites. The comparison is nevertheless limited by the use of clean, static surfaces. Particle size, metal-support interfaces, steam and coke coverage, and redox restructuring are absent from most models.

3.2 CaO-Based Catalysts

Previous calculations treated the interaction between CaO and pre-formed tar radicals using molecular models. These calculations showed exothermic adsorption and reduced C-C bond populations, but they did not determine a complete surface reaction pathway. Periodic surface models subsequently allowed transition states and metal-doping effects to be examined more directly.

Chen *et al*. used B3LYP/6-31G (d,p) calculations to examine the adsorption of benzene-, toluene-, and phenol-derived radicals on CaO[28]. Their results showed that adsorption of tar radicals on CaO-based catalysts is exothermic and reduces the stability of key C-C and C-H bonds, with C-H cleavage being favored as the initial step and subsequently facilitating C-C bond cleavage. The catalytic activity of the CaO-based system also differs markedly among the three tar components, following the order phenol > benzene > toluene. Thus, the role of CaO-based catalysts in tar removal extends beyond simple adsorption and enrichment, instead involving direct weakening of critical intramolecular bonds through interactions between the basic surface and tar molecules, thereby promoting subsequent cracking.

Wang *et al*. compared CaO, Ni/CaO, Fe/CaO and Ni-Fe/CaO using toluene as the tar model compound[27]. The DFT calculations predicted the adsorption-strength order Fe/CaO < CaO < Ni/CaO < Ni-Fe/CaO. Consistently, fixed-bed experiments conducted at 650 °C showed that Ni-Fe/CaO gave 98.11% toluene conversion and a 93.11% H_2 yield. Relative to Ni/CaO, the H_2 yield increased by 27.92%, whereas the CH_4 yield decreased by 50.43%. Thermogravimetric analysis also indicated less carbon deposition on Ni-Fe/CaO. The experimental product distribution is therefore consistent with the calculated preference for H_2 formation.

More recently, Wei *et al*. further explained Ni- and Fe-doped CaO from the view of surface electronic structure[32]. Using benzene, phenol and toluene, they compared adsorption, electronic properties and initial cracking on CaO, Ni-doped CaO and Fe-doped CaO. Ni or Fe doping increased electron affinity and conductivity, strengthened Ni/Fe d and O p orbital interactions, and improved tar adsorption and activation. For toluene, methyl C-H activation remained the preferred initial step, while Ni- and Fe-doped CaO lowered the barrier by 15.70% and 21.70%, respectively. Metal doping therefore promotes cracking through electron redistribution, orbital hybridization and intermediate stabilization[27,32].

Overall, pure CaO-based catalysts mainly rely on surface basicity to weaken bond stability in tar molecules, whereas incorporation of metals such as Ni and Fe further promotes tar cracking and conversion toward H_2/CO through electronic-structure regulation and intermediate stabilization[27,28,32].

3.3 Carbon-Based Catalysts

Compared with ideal metal single-crystal surfaces, carbon-based catalysts, often containing metal nanoparticles, defects, and oxygen functionalities, better resemble real conversion environments and regulate tar cracking, reforming, and coking[29,30].

Du *et al*. performed DFT analyses on the reaction behavior on the surface of biochar-supported Ni nanoparticles using toluene as a model compound[29]. The results showed that toluene adsorbs preferentially in a parallel configuration, with stronger adsorption at step sites than at terrace sites. The biochar support helps disperse Ni particles and stabilize more low-coordination interfacial Ni sites, which promotes the initial activation of tar molecules. Subsequent reactions proceed through methyl dehydrogenation, aromatic C-H cleavage, and ring opening, eventually yielding smaller hydrocarbon fragments. The combined experimental and computational results associate the higher activity with smaller Ni particles and a larger proportion of corner and step sites.

Qian *et al*. compared biochar-supported Ni catalysts prepared from $Ni(NO_3)_2$, $NiCl_2$ and $NiSO_4$ during microwave-assisted steam reforming of toluene at 650 °C[30]. Characterisation identified metallic Ni in all three catalysts, whereas part of the Ni in the $NiSO_4$-derived catalyst was present as Ni_3S_2. DFT calculations indicated that metallic Ni weakened the methyl C-H bond and the adjacent C-C bond in toluene more effectively than Ni_3S_2. This difference was consistent with the lower cracking activity of the

Ni_3S_2-containing catalyst. The $Ni(NO_3)_2$-derived catalyst retained 81.60% toluene conversion after 190 min and showed better resistance to carbon deposition. Catalyst stability also depended on the steam-to-carbon ratio, as excessive steam damaged the carbon matrix and accelerated deactivation. The static Ni and Ni_3S_2 models did not include microwave heating or the gradual changes in the biochar support during reaction.

These studies suggest that the carbon framework does more than simply support the metal phase. By affecting metal dispersion, tar adsorption, initial dehydrogenation, and coking behavior, it may help tar enter reforming pathways at lower temperatures.

3.4 External-Field-Assisted Simulations

External-field evidence in DFT studies of biomass tar conversion remains narrow. The clearest DFT-experimental case is magnetic-field regulation of phenol cracking over Ni/CaO-$Ca_{12}Al_{14}O_{33}$. Evidence for electric- or microwave-field effects on elementary tar-conversion steps is not yet comparable.

Wang *et al*. examined phenol cracking over Ni/CaO-$Ca_{12}Al_{14}O_{33}$ under magnetic fields of 0 mT and 80 mT[31]. The field altered charge transfer and the electronic structure of the Ni sites. Among the calculated elementary steps, ring opening showed the largest change in barrier, decreasing from 1.23 eV to 0.85 eV. The barriers for hydroxyl dehydrogenation, aromatic C-H cleavage, and subsequent ring cleavage changed less markedly. As shown in **Table 3**, the comparison of transition-state energies under 0 mT and 80 mT further demonstrated that magnetic-field regulation can alter the phenol cracking pathway at the catalytic interface. Consistently, experimental results showed that, at 700 °C and 80 mT, phenol conversion reached 98.70%, while H_2 and CO yields increased by 25.10% and 60.70%, respectively, and CO_2 emissions decreased by 37.50%.

Table 3. Transition states of phenol cracking elementary reactions

Elementary Reaction Step	Reaction Process	Transition State	Energy Barrier at 0 mT / eV	Energy Barrier at 80 mT / eV	Decrease / eV	Decrease / %
Step 1	Hydroxyl dehydrogenation	TS1	1.83	1.66	0.17	9.30
Step 2	C-H bond dehydrogenation	TS2	3.39	3.22	0.17	5.00
Step 3	Benzene ring opening	TS3	1.23	0.85	0.38	30.90
Step 4	Ring cleavage	TS4	2.49	2.43	0.06	2.40

This study extends DFT research on tar removal from conventional catalyst-composition design to magnetic-field regulation. It suggests that the magnetic field can change the electronic structure of catalytic interfaces, which may further affect phenolic tar conversion and syngas production. However, current external-field-assisted DFT studies are still limited, and more work is needed to clarify how field strength, spin-dependent electron transfer, multicomponent tar adsorption, and catalyst evolution influence the reaction under realistic pyrolysis conditions.

Tar-removal performance is not determined by the lowest cracking barrier alone. The useful interface is the one that can activate the relevant tar fraction and still remove the carbon left by that activation. Ni-rich sites are effective for C-H activation and reforming, but they need steam, CO_2 or an oxygen-supplying support to avoid carbon accumulation. CaO-containing systems are better suited to cases where tar cracking is coupled with H_2 formation or CO_2 regulation, although carbonation and loss of basicity limit what can be inferred from ideal models. Biochar-supported metals are closer to biomass operation, but their active sites are harder to define because metal particles, defects, oxygenated groups, and ash species evolve together. DFT should therefore be used to test whether a proposed interface can sustain both tar activation and carbon removal, not to rank catalyst families from isolated barriers.

4. DFT Research on Bio-Oil Upgrading

Bio-oil from fast pyrolysis contains water and various oxygenated compounds, including phenols, furans, carbonyls, carboxylic acids and esters. These components are responsible for its low heating value, corrosiveness and poor storage stability, making upgrading necessary before further utilization. In DFT studies, phenol, guaiacol, furfural and HMF are commonly used to represent the main phenolic and furanic fractions of bio-oil. These models make it possible to compare elementary deoxygenation steps on metal, carbide, oxide and supported catalysts, but the calculated pathway depends strongly on the chosen molecule, surface structure and reaction environment. This section reviews DFT studies of phenolic and furanic hydrodeoxygenation (HDO), with emphasis on how calculated pathways explain deoxygenation selectivity. **Table 4** summarizes the representative model compounds and catalyst/interface models discussed in this section.

Table 4. Representative DFT model systems for bio-oil upgrading

Bio-Oil Model Family	Representative Compounds	Catalyst / Interface Models	Main DFT Focus
Phenolic Monomers	Phenol, guaiacol	Pt(111), Pt clusters, Fe surfaces, Ru/water interfaces	C-O cleavage, dehydroxylation, demethoxylation and ring hydrogenation
Lignin-Derived Phenolic Dimers	β-O-4 dimers, PPE-type models	Ru(0001), Ru/Nb_2O_5 and supported Ru interfaces	Ether-linkage cleavage and oligomer-relevant hydrodeoxygenation (HDO) pathways
Furanic Oxygenates	Furfural, furfuryl alcohol, HMF	Ni(111), FeNi, Mo_2C, Co/Mo_2C and M/Pt surfaces	C=O/C-OH conversion, decarbonylation, ring opening and hydrogenation
Interface / Solvent / ML-Assisted Systems	Furfural, HMF and related intermediates	Co@CoO, Ni-ZnO/AC, Cu-Re-O_x, CoCr/ PdMo/ PdW screening	Active hydrogen, solvent-mediated transfer and descriptor-based catalyst screening

NOTE: HDO: hydrodeoxygenation; HMF: 5-hydroxymethylfurfural; ML: machine learning; PPE: 2-phenylethyl phenyl ether.

4.1 Phenolic Model Compounds

Phenolic compounds are commonly represented by phenol, guaiacol, and lignin-derived ether models in DFT studies of bio-oil upgrading. Their HDO is not governed by a single deoxygenation step, but by competition among aromatic-ring hydrogenation, dehydroxylation, demethoxylation and direct C-O bond cleavage. This competition is sensitive to the coordination environment of the active site. Lu *et al*. constructed a guaiacol reaction network on Pt(111), including hydrogenation, dehydrogenation and decomposition steps[33]. Their microkinetic analysis indicated that flat Pt(111) terraces favor hydrogenation-related pathways, whereas direct removal of oxygen-containing groups is much less favorable. In contrast, Nania *et al*. used a subnanometric Pt_{10} cluster and reported that direct C(sp^2)–O cleavage can become kinetically more favorable than deoxygenation after aromatic-ring hydrogenation[34]. These two studies do not constitute a strictly controlled comparison, because the surface models, reaction networks, and computational settings are different. Taken together, however, they suggest that the predicted HDO selectivity is sensitive to site coordination. A clean terrace is therefore useful as a reference surface for elementary-step analysis, but it should not be directly extrapolated to supported nanoparticles, where low-coordinated atoms, particle size and metal-support contacts may alter the balance between ring hydrogenation and C-O cleavage.

Metal-oxygen interactions are often used to rationalize phenolic deoxygenation, but existing calculations do not support a universal activity order based on oxygen affinity alone. A surface must interact sufficiently with the oxygenated group to orient the adsorbate and polarize the C-O bond, but overly strong stabilization of oxygenated intermediates or oxygen-derived surface species may hinder oxygen removal or contribute to site blocking under sufficiently high oxygen coverage. Fe-containing and Ru-based systems illustrate this point. On Fe-based surfaces, the interaction between the metal site and the oxygenated functional group can promote dehydroxylation or C-O activation, whereas the pathway still depends on hydrogen participation and surface state[35,36]. For Ru-based catalysts, deoxygenation is also affected by the way oxygenated intermediates bind at both metal–water boundaries[37,38] and metal-support contacts[39]. Therefore, "oxygen affinity" should be specified by the actual calculated quantity, such as adsorption energies of phenoxy, methoxy, or other oxygenated intermediates, C-O cleavage barriers, surface oxygen binding energies or oxygen-removal thermodynamics. These quantities are related, but they should not be merged into a single descriptor without identifying the elementary step or adsorbed state being discussed.

The identity of active hydrogen further complicates phenolic HDO. Surface H atoms, hydride-like species, interfacial protons and water-derived hydroxyl groups are not equivalent because they participate in different hydrogenation, hydrogenolysis and proton-transfer steps. Hensley *et al.* compared direct dehydroxylation, hydrogen-assisted dehydroxylation and tautomerization of phenol on Fe(110), and further introduced water into the model[35]. The presence of water changed both proton-transfer energetics and the hydroxylation state of the surface, thereby altering the preferred dehydroxylation route relative to the vacuum surface. For Ru-water systems, the role of water has been clarified more directly. In the H_2O-Ru(0001) model, water opened a lower-energy C-OCH_3 cleavage route through proton transfer to the methoxy oxygen, reducing the barrier by up to 0.8 eV compared with the unassisted route[37]. Shangguan *et al*. further showed that guaiacol hydrogenolysis at the Ru nanoparticle-water interface involves the coupled action of interfacial protons and hydride-like species; alternative direct C-OCH_3 cleavage routes were calculated to require at least 22 kJ·mol^{-1} higher effective activation free energies than the proposed proton/hydride-mediated route[38]. The mechanistic consequence is model-specific: introducing water changes not only the barrier of a given step, but also the identity of the reactive interfacial species. Thus, the lowest-barrier pathway on a dry metal surface should not automatically be taken as the dominant route under liquid-phase or water-containing HDO conditions.

Phenolic model compounds have also been extended from monomers to lignin-derived ether structures. Wen *et al*. used 2-phenylethyl phenyl ether (PPE) as a β-O-4 model compound and combined DFT calculations with HDO experiments over Ru-based catalysts[39]. Ru(0001) was used to analyze PPE adsorption and β-O-4 cleavage, while Ru/Nb_2O_5 was tested for both PPE and lignin-derived bio-oil upgrading. This model is closer to lignin-derived oligomeric components than phenol or guaiacol, but it still represents only one ether linkage and cannot reproduce the full distribution of lignin-derived phenolic monomers, dimers and heavier oligomers. The experimental performance of supported Ru catalysts supports the relevance of interfacial effects in phenolic HDO, but it does not by itself prove that a single calculated transition-state pathway is uniquely responsible for real bio-oil upgrading.

Collectively, these studies suggest that phenolic HDO cannot be described by a universal pathway or by a single oxygen-affinity descriptor. Its predicted selectivity instead depends on the coupling among site coordination, adsorption configuration and the mode of hydrogen delivery. The transferability of this conclusion nevertheless remains limited by differences in solvent treatment, hydrogen coverage and the structural complexity of the phenolic model.

4.2 Furanic Model Compounds

Furanic model compounds, including furfural, furfuryl alcohol and HMF, are representative of carbohydrate-derived oxygenates and their upgrading intermediates. Their hydrodeoxygenation differs from phenolic HDO because the desired conversion usually starts from exocyclic C=O or C–OH groups rather than from the furan ring itself. The main selectivity problem is therefore to promote selective hydrogenation and hydrogenolysis of the exocyclic oxygenated groups while suppressing decarbonylation, furan-ring opening, and deep hydrogenation. In this context, DFT is useful not only for comparing individual activation barriers, but also for identifying which bond becomes preferentially activated under a given adsorption geometry and interfacial environment.

Adsorption geometry is a recurring mechanistic variable in DFT studies of furanic HDO. Yu *et al*. used furfural as a model molecule and compared its adsorption and conversion on Ni(111), monolayer FeNi(111) and FeNi alloy surfaces[40] Fe strengthened the interaction with the carbonyl oxygen, polarized the C=O bond and tilted the furan ring away from the surface, which was associated with preferential conversion through the exocyclic carbonyl group rather than direct activation of the ring. Similar structure-selectivity relationships have been discussed for carbide and bimetallic surfaces. Lin *et al*. showed that furfural adsorbed on Mo_2C(0001) and Co/Mo_2C(0001) through an η^2(C, O) configuration, which elongated the exocyclic C=O bond and facilitated its subsequent transformation[41]. Co modification did

not simply increase HDO activity; rather, it weakened the binding of adsorbed oxygen species and furfural compared with bare Mo_2C, thereby improving resistance to surface oxygen accumulation and catalyst deactivation. Combined TPD, high-resolution electron energy-loss spectroscopy (HREELS) and flow-reactor evidence was consistent with this interpretation: Mo_2C and Co/Mo_2C showed similar initial 2-methylfuran selectivity, but Co/Mo_2C exhibited markedly better stability. Jiang *et al*. further compared M/Pt(111) bimetallic surfaces (M = Cu, Ni, Fe, Co) for furfural HDO[42]. Co- and Fe-terminated surfaces exhibited stronger furfural binding and greater furan-ring tilting, and the experimental 2-methylfuran yield followed the order Co > Fe > Ni > Cu, whereas furan formation showed the opposite trend. These studies collectively suggest that η^2(C, O) adsorption, C=O elongation and ring-tilting configurations are consistently associated with preferential activation of the exocyclic oxygenated group. However, this relationship should be treated as a model-dependent correlation unless the effect of geometry is isolated through controlled calculations.

Active hydrogen, oxygen vacancies and solvent-mediated hydrogen transfer further affect whether the activated C=O or C-OH group undergoes selective HDO or a competing pathway. Xiang *et al*. showed that oxygen vacancies in the CoO shell of Co@CoO facilitated both heterolytic and homolytic H_2 dissociation, producing hydride-like $H^{\delta-}$ species that participated in C-O bond cleavage during HMF hydrogenolysis[43]. This example shows that surface H, hydride-like hydrogen and protonic species should not be treated as interchangeable hydrogen sources. The reaction environment can also alter the effective hydrogen-transfer pathway. Huang *et al*. reported solvent-regulated HMF hydrogenation over Ni-ZnO/AC[44]. In 1,4-dioxane, HMF was mainly converted to 2,5-bis (hydroxymethyl)furan (BHMF), whereas in isopropanol (iPrOH), 2,5-dimethylfuran (DMF) formation was favored; the reported BHMF and DMF selectivities reached 97.50% and 99.50%, respectively. Their DFT calculations indicated that the activation energy for the key BHMF-to-5-methylfurfuryl alcohol (MFA) step decreased from 1.07 eV in 1,4-dioxane to 0.60 eV in iPrOH, consistent with a hydrogen-shuttle role of the protic solvent. This result supports solvent-assisted pathway regulation, but it does not constitute a complete representation of liquid-phase, multicomponent bio-oil upgrading. Cu-Re-O_x interfaces provide another interfacial case: operando-FTIR and DFT calculations indicate that furfural conversion to 2-methylfuran proceeds through a dehydroxylation pathway at Cu-Re-O_x-rich interfaces[45]. Together, these studies indicate that furanic HDO depends not only on adsorption strength, but also on the identity of the hydrogen species delivered to the oxygenated group and on the ability of the interface to facilitate oxygen removal without excessive carbon loss or ring destruction.

Active learning is a data-efficient machine-learning strategy in which a surrogate model iteratively selects informative candidates for additional DFT calculations. Deng *et al*. applied a DFT–active learning workflow to a space of 223 bimetallic catalysts, using surface energy and the C-O bond-cleavage barrier as stability- and activity-related targets, respectively[46]. The analysis identified the mean d-band center and mean Mendeleev number as influential descriptors and prioritized CoCr, PdMo, and PdW, for which DFT predicted C-O cleavage barriers of approximately 0.20 eV. CoCr was subsequently tested experimentally, giving 98.10% furfuryl alcohol conversion and 97.90% 2-methylfuran selectivity under the reported conditions. The main advantage of this approach is that it directs expensive DFT calculations toward informative regions of a large compositional space while providing descriptor-based candidate ranking.

However, this case demonstrates catalyst prioritization rather than direct product-selectivity prediction, because the machine learning (ML) targets do not represent competing reaction pathways. Its transferability is also limited by the size and chemical diversity of the training data, the consistency of the DFT labels, the selected descriptors and surface models, and the omission of coverage, solvent, and catalyst-reconstruction effects. Reliable selectivity prediction will require competing free-energy pathways, uncertainty quantification, microkinetic modelling, and experimental validation.

Comparison of phenolic and furanic model compounds indicates that bio-oil HDO involves shared controlling variables but not a common selectivity logic. Phenolic HDO networks may involve direct aryl-O cleavage, demethylation/demethoxylation and hydrogenation-assisted pathways, so the key issue is to identify which route removes oxygen while limiting aromatic-ring saturation and carbon loss. The predicted selectivity depends jointly on adsorption geometry, including flat π-bound and O-bound configurations, and on whether adsorption occurs at terrace, low-coordinated or interfacial sites. Furanic HDO, by contrast, usually starts from exocyclic C=O or C-OH groups, while decarbonylation, ring opening and deep hydrogenation are the main competing routes. In this case, η^2(C, O) adsorption, furan-ring tilting and the orientation of the exocyclic oxygenated group are associated with preferential activation of the exocyclic functionality rather than the furan ring. In the studies considered here, phenolic systems particularly highlight proton-hydride cooperation at water-metal interfaces, whereas furanic systems more often emphasize vacancy-assisted H_2 activation and solvent-mediated hydrogen transfer to exocyclic groups. Across both families, oxygen binding, adsorption geometry and hydrogen delivery are shared variables, but their mechanistic significance remains substrate-dependent.

Comparison of phenolic and furanic model compounds indicates that bio-oil HDO involves a shared mechanistic framework but substrate-dependent selectivity. In both families, deoxygenation is controlled by the coupling of oxygenate adsorption, hydrogen activation and delivery, C–O bond cleavage or oxygen removal, and the desorption of surface oxygen species. Phenolic HDO may proceed through direct aryl–O cleavage, demethylation or demethoxylation, dehydroxylation, and hydrogenation-assisted pathways, with oxygen removal competing against aromatic-ring saturation and carbon loss. Furanic HDO, by contrast, generally involves initial activation or hydrogenation of exocyclic C=O or C–OH groups, followed by hydrogenolysis, while decarbonylation, ring opening, and deep hydrogenation remain the principal competing pathways. Thus, oxygen binding, adsorption geometry, and hydrogen delivery are common controlling variables, but no universal initial step or selectivity descriptor can be transferred directly between the two oxygenate families.

Accordingly, a general catalyst-regulation strategy should not aim simply to maximize oxygen affinity. Effective HDO interfaces should combine moderate oxygen binding, substrate-selective adsorption geometry, and a mode of hydrogen delivery matched to the target bond-breaking step. For phenolic oxygenates, low-coordinated metal sites or metal-water and metal-support interfaces should facilitate aryl–O, alkoxy C–O, or ether-linkage cleavage while limiting excessive aromatic-ring hydrogenation.

For furanic oxygenates, the exocyclic C=O or C–OH group should be oriented toward the active site while interaction of the furan ring with the surface is restricted; the interface should also activate hydrogen efficiently and remove surface oxygen before site blocking occurs. The transferability of these principles nevertheless requires verification under realistic solvent, hydrogen-coverage, coadsorption, and reconstructed-interface conditions. Isolated adsorption energies or C–O cleavage barriers should therefore be used to formulate testable catalyst-design hypotheses rather than universal activity rankings.

5. DFT Studies on Syngas Conditioning in Pyrolysis-Derived Biomass Conversion

The gases released during biomass pyrolysis and gasification do not become a stable product stream immediately after primary decomposition and tar formation. CH_4, CO, CO_2, H_2O and H_2 coexist with tar fragments, char, coke and ash-derived species, and continue to undergo reforming, carbon gasification and water-gas shift reactions. The key issue is how carbon activation, oxygen transfer and active-site regeneration together determine H_2/CO, carbon conversion and catalyst deactivation.

DFT can resolve elementary pathways in this process, but a calculated barrier is meaningful only within the model used. Surface carbon (C^*) is not equivalent to tar-derived coke or heterogeneous biomass char, and a clean metal-oxide surface does not include competitive adsorption by CO, H_2O, CO_2 and aromatic species.

5.1 Methane and Tar Reforming Coupled with Carbon Removal

On Ni/CeO_2 catalysts, Lustemberg *et al*. correlated methane conversion with Ni coverage and DFT models, identifying small cationic Ni clusters at ceria step edges as favourable sites for the first C–H activation[47]. Salcedo *et al*. further combined ambient-pressure X-ray photoelectron spectroscopy with DFT and showed that water dissociation occurs readily at the Ni-CeO_2 perimeter[48]. The resulting OH species open a lower-energy route for carbon oxidation through a COH intermediate, whereas direct oxidation by ceria lattice oxygen requires a much higher calculated barrier of 2.17 eV. These results indicate that methane activation alone is not a sufficient descriptor. Sustained reforming also requires water activation, oxygen transfer and removal of carbonaceous intermediates before the active interface is blocked.

In biomass conversion, carbon can appear as adsorbed C^*, tar-derived coke, biochar surface carbon or mineral-containing char. These species are chemically related but not interchangeable. Zou *et al*. represented biomass char by oxygen-containing aromatic boundaries and found that steam gasification depends on boundary structure and oxygen migration[49]. Zhao and Zhang used a toluene/biochar model to examine carbon formation during tar decomposition and its subsequent removal by H_2O or CO_2[50]. Their calculations linked continued tar conversion to oxidant-assisted removal of deposited carbon. However, the apparent preference between H_2O- and CO_2-assisted pathways depends on the selected char model and active site. It should not be generalized to all biomass chars, catalyst coke, or idealized surface C^*.

Guizani *et al*. found that H_2O and CO_2 gasified beech-wood char through different routes, while their mixture produced both competitive and synergistic effects[51]. Isolated H_2O and CO_2 pathways therefore cannot simply be ranked and extrapolated to mixed-feed gasification. Carbon reactivity is also altered by pore structure, surface oxygen groups and inorganic constituents. During in situ corn-straw tar reforming, the activity followed the order sawdust biochar > coal char > graphite, consistent with the combined effects of carbon structure and alkali and alkaline-earth metals[52]. Experiments and DFT for sawdust-char CO_2 gasification gave the order KCo > KNi > KFe > KCe and distinguished metal-mediated oxygen transfer from a ceria-vacancy cycle[53]. High-temperature in situ DRIFTS, isotopic-water experiments and molecular simulations further assigned spectral features to K-promoted char-polyynes during cellulose-char gasification[54]. These results do not invalidate ideal carbon-edge models. Rather, they specify the chemical features that such models omit.

Across these studies, CH_4 dissociation alone is not a sufficient descriptor. Activity depends on the balance among H_2O/CO_2 activation, formation of C-O or C-OH species, stability of the carbonaceous intermediate, and regeneration of the interfacial site. The relative importance of these factors changes with carbon structure, mineral content and gas composition. A catalyst predicted to cleave C-H bonds readily may therefore still deactivate if oxygen transfer or carbon removal is slow.

5.2 WGS/RWGS under Evolving Interfacial Conditions

WGS and RWGS reactions regulate H_2/CO in a gas composition that is already being changed by methane reforming, tar reforming and carbon gasification. CO is not only a product; it can also block active sites. H_2O-derived OH species, lattice oxygen and oxygen vacancies can participate in several competing steps. For this reason, WGS/RWGS should not be treated only as independent reactions added after reforming, but as part of the same interfacial oxygen-transfer network.

Ding *et al*. used CO-probe infrared spectroscopy to distinguish Pt single atoms from Pt nanoparticles and showed that Pt nanoparticles are the active sites for low-temperature CO oxidation and WGS, whereas isolated Pt atoms bind CO too strongly and behave mainly as spectators[55]. Li *et al*. further showed on Pt/CeO_2 that active sites can form and reorganize under WGS conditions, with in situ microscopy and spectroscopy revealing dynamic Pt species and ceria-associated interfacial sites[56]. These studies show that adsorption stability on a predefined model site is not enough to identify the working catalyst.

For RWGS, Chen *et al*. used DFT+*U* and microkinetic modelling to examine an isolated Ru atom on CeO_2(111)[57]. The calculated network suggested that the dominant low-temperature active structure is not the initial RuO_3 species, but a hydroxylated $Ru(OH)_3$-(OH) configuration formed through hydrogen spillover. At higher temperature, oxygen vacancies become more accessible and a Mars-van Krevelen-type route becomes more important. This result is valuable because it links rate control to temperature, hydrogen coverage and support reduction. It should not, however, be directly extrapolated to biomass-derived syngas without considering tar fragments, ash species, coke precursors and coverage effects.

Thus, the main lesson from WGS/RWGS studies is not that one metal or one site is universally optimal. The more important point is that H_2/CO regulation depends on a changing interface, where CO adsorption, OH/O transfer, vacancy formation and metal-support restructuring occur together. DFT can identify plausible pathways within a defined model, but experimentally constrained and coverage-aware models are needed before those pathways can be used for process-level prediction.

5.3 Coupling and Rate Control in the Integrated Reaction Network

A more biomass-specific use of DFT is to place reforming, carbon removal and WGS/RWGS within the same catalytic-pyrolysis network. Wang *et al*. provided one of the few DFT-based comparisons of multiple gas-conditioning reactions within a common biomass catalytic-pyrolysis system[58]. Their Ni/CaO and Ni-Fe/CaO models included toluene cracking, methane steam reforming, dry reforming, WGS, the water-carbon reaction and the Boudouard reaction. The corresponding experiments were consistent with enhanced gas formation. At 650 °C, Ni-Fe/CaO reduced the liquid yield by 18.32%, increased the gas yield by 26.27% and raised the H_2 yield by 18.29% to 453.34 mL g^{-1} biomass relative to Ni/CaO.

NC denotes Ni/CaO, NFC denotes Ni–Fe/CaO, and rate determining step (RDS) denotes the rate-determining step. The reactions are network modules used in that study rather than a complete description of biomass-derived gas chemistry.

Table 5 shows that Fe incorporation did not alter every assigned RDS. The assignments for toluene cracking, WGS, the water-carbon reaction and the Boudouard reaction remained unchanged. The RDS identity changed only for the two methane-reforming modules in the reported model. It shifted from CH_3 dehydrogenation to $CO_2 + H \rightarrow COOH$ in dry reforming, and to $CHO \rightarrow CO + H$ in steam reforming.

Table 5. The biomass catalytic pyrolysis network system[58]

Chemical Equation	RDS (Rate Determining Step)	
	NC (Ni/CaO)	NFC (Ni–Fe/CaO)
$C_7H_8 \rightarrow 2H_2 + CH_4 + 6C$ (Tar Cracking and Carbon Entry)	$C_7H_8 = C_6H_5 + CH_3$ 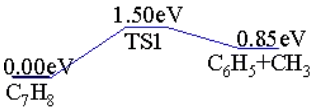	$C_7H_8 = C_6H_5 + CH_3$ 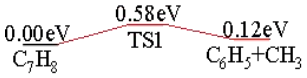
$CO + H_2O \rightarrow CO_2 + H_2$ (WGS and H_2 Regulation)	OH = O + H 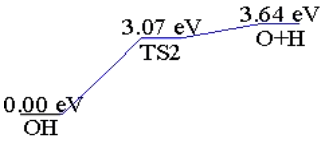	OH = O + H 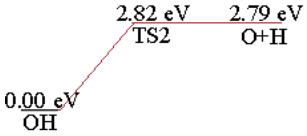
$CH_4 + CO_2 \rightarrow 2CO + 2H_2$ (Dry Reforming)	$CH_3 = CH_2 + H$ 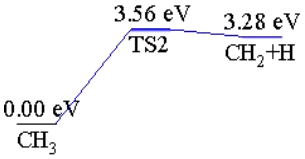	$CO_2 + H = COOH$ 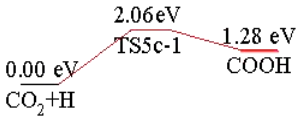
$CH_4 + H_2O \rightarrow CO + 3H_2$ (Steam Reforming)	$CH_3 = CH_2 + H$ 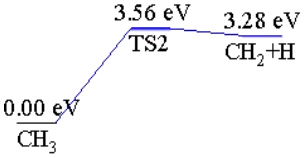	$CHO = CO + H$ 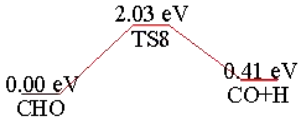
$C + H_2O \rightarrow CO + H_2$ (Water-Carbon Reaction)	$H_2O = OH + H$ 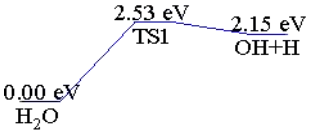	$H_2O = OH + H$ 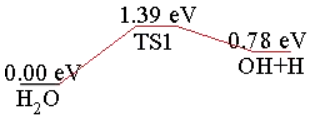
$C + CO_2 \rightarrow 2CO$ (Boudouard Reaction)	$CO_2 = CO + O$ 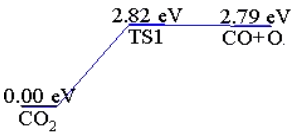	$CO_2 = CO + O$ 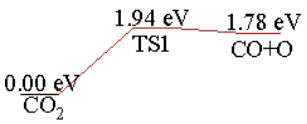

For the NFC system, the WGS module retained the largest reported RDS barrier, followed by dry reforming and steam reforming[58]. In the NC system, however, the highest barriers were associated with the reforming modules rather than WGS. Fe incorporation therefore altered both the magnitude and ordering of the dominant kinetic constraints.

Overall, syngas conditioning should be interpreted as a coupled reaction network rather than as separate reforming, carbon-removal and WGS/RWGS steps. CH_4 activation, H_2O/CO_2 dissociation, carbon oxidation and OH/O transfer share active sites and intermediates, so isolated barriers cannot by themselves predict H_2/CO ratio, carbon efficiency or coke resistance. Gas-yield measurements, coke analysis, isotope tracing and operando spectroscopy can constrain the proposed active sites and carbon-

removal routes, but they still do not provide a complete coverage-dependent flux map for biomass-derived gas mixtures. The most useful DFT outputs are therefore mechanistic links between carbon entry, oxygen delivery, active-site regeneration and measurable syngas quality.

6. Future Prospects

Although DFT has provided molecular-level insights into biomass thermochemical conversion, most studies relied on simplified models, idealized surfaces, and isolated elementary steps to study the catalytic mechanism. In order to make the simulation more consistent with real conditions, future research may focus on three interconnected methodological directions: reaction-network analysis, realistic catalytic models, and ML-assisted prediction, as summarized in **Figure. 2**. The translation of molecular mechanisms into engineering guidance is discussed separately in Section 6.4.

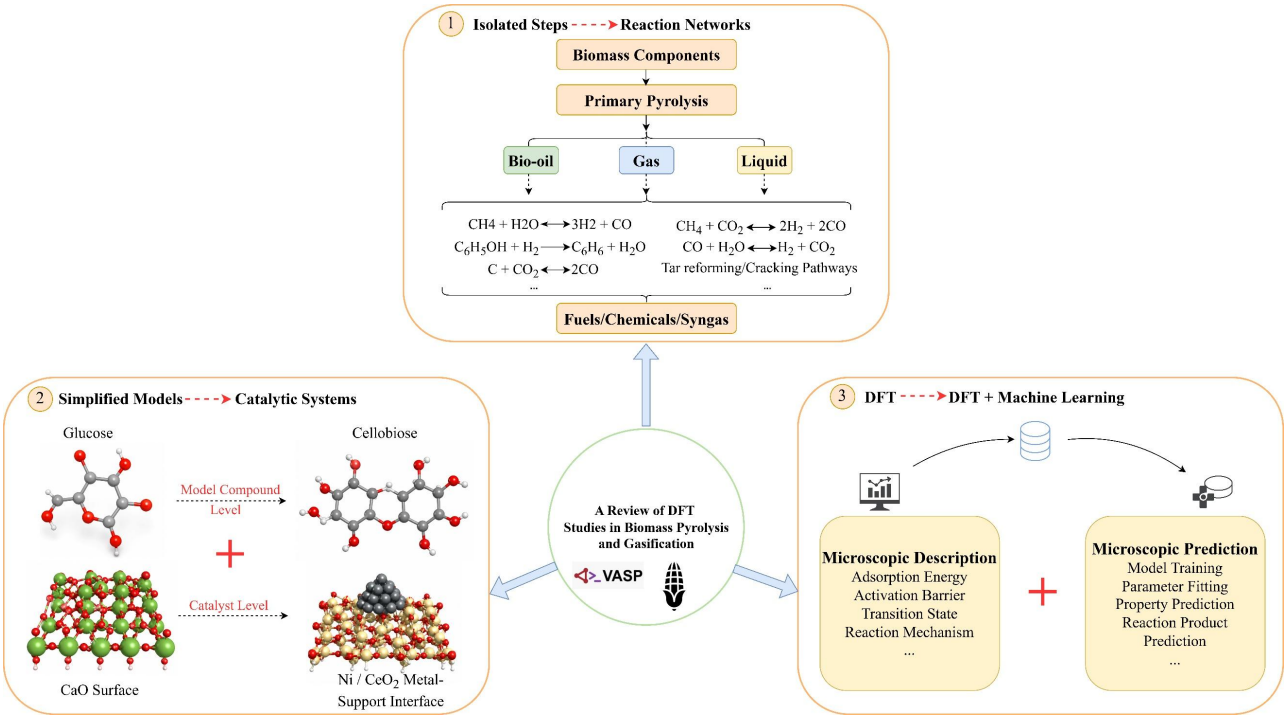

Figure.2 Future directions in DFT-assisted biomass thermochemical conversion. (1) Isolate steps toward reaction network analysis; (2) Simplified models toward realistic catalytic systems; (3) DFT toward DFT+ machine learning. **NOTE:** DFT: Density Functional Theory. Copyright: The figure was created by the authors using draw.io (diagrams.net, web version 30.3.13).

6.1 Toward Reaction-Network Analysis

A more useful role for DFT is to identify which molecular steps actually control the evolution of carbon, hydrogen and oxygen during biomass conversion. At present, many studies still discuss primary pyrolysis, tar cracking, bio-oil upgrading and syngas conditioning as separate reactions. In practice, these stages are coupled. Oxygenates and phenolic fragments from primary pyrolysis may become tar, undergo deoxygenation, reform into light gases or participate in coke formation. Likewise, CH_4 reforming, WGS/RWGS and carbon-removal reactions share surface C, CH_x, O, OH and H species. Therefore, a low activation barrier for one isolated step is not enough to explain product distribution or catalyst performance.

Future DFT work should place elementary reactions within a kinetic network. Adsorption energies and transition-state barriers need to be connected with microkinetic modelling, kinetic Monte Carlo simulation or coverage-dependent analysis, so that rate-controlling steps can be distinguished from pathways that are merely thermodynamically possible. This is particularly important for evaluating tar suppression, coke resistance, oxygen-removal efficiency and H_2/CO regulation.

6.2 Toward Realistic Catalytic Models

The limitation is most evident for lignin. β-O-4 dimers explain primary cleavage and phenolic-monomer formation, but real lignin also contains β-5, β-β, 5-5 and 4-O-5 linkages. These condensed structures are closely related to secondary radical coupling, phenolic oligomerization, heavy tar formation and char precursors. Future DFT studies should therefore pay more attention to substituted and condensed lignin fragments, not only to the most convenient β-O-4 model.

Catalyst models also need to approach working interfaces. Clean single-crystal surfaces and single-adsorbate calculations are useful starting points, but biomass conversion involves steam, CO_2, H_2, CO, tar mixtures, oxygenates, ash, alkali metals and coke precursors. More realistic calculations should include co-adsorption, surface coverage, oxygen vacancies, metal-support interfaces, biochar defects and reconstructed active sites. For oxides and defective catalysts, the influence of functional choice, dispersion correction, spin state and free-energy correction should also be checked before small barrier differences are used to support broad mechanistic conclusions.

6.3 Toward ML-Assisted Prediction

ML utilizes big data and algorithmic models to build mapping relations via sample training for property and product prediction. Machine learning can assist DFT in preliminary screening of structures and models, thereby reducing invalid calculations.

Biomass thermochemical conversion contains too many feedstock fragments, catalyst compositions, surface defects and secondary reactions for one-by-one DFT screening. The microscale DFT mechanism combined with macroscale machine learning forms a multi-scale simulation system, which is highly suitable for research in the field of biomass catalytic thermochemical conversion.

A useful DFT-ML workflow should be closed by kinetics and experiment, not by screening alone. Low-barrier candidates are meaningful only if the predicted step can influence carbon, hydrogen or oxygen transfer under working conditions. Kinetic modelling can test whether this connection is plausible, while isotope labelling, operando spectroscopy, TPD/temperature-programmed surface reaction (TPSR), Py-GC/MS, TG-FTIR and high-resolution mass spectrometry can relate calculated pathways to observable gases, vapours, surface species and oligomeric products. Experiments therefore do more than confirm DFT predictions; they define the range within which calculated barriers and descriptors remain defensible. For biomass-derived solid wastes, this validation loop is ultimately valuable only when it improves engineering decisions, suppressing tar carryover, slowing coke formation, regulating H_2/CO, increasing carbon utilization and extending catalyst lifetime under variable feedstock and operating conditions.

6.4 From Molecular Mechanisms to Engineering Guidance

The engineering value of DFT will ultimately depend on whether molecular-scale energetics can be translated, through kinetic and reactor models, into measurable process targets and controllable operating variables. For biomass pyrolysis, reaction pathways and activation barriers derived from representative cellulose, hemicellulose and lignin structures can help identify the temperature-sensitive bond-cleavage and secondary condensation routes governing the formation of gases, condensable oxygenates, tar and char. When incorporated into microkinetic and reactor-scale models, these data could constrain operating windows for improving carbon conversion, suppressing heavy-tar and char-precursor formation, and promoting clean valorization while reducing the fraction of waste biomass requiring final disposal. For tar removal, DFT can identify catalyst compositions and interfacial structures that balance aromatic activation and reforming with steam- or CO_2-assisted oxidation of deposited carbon and active-site regeneration. Such information could inform catalyst selection and optimisation of the reaction atmosphere, thereby mitigating tar condensation, reactor fouling, pipeline blockage, catalyst deactivation and associated corrosion risks. In bio-oil upgrading, calculated competition among C-O cleavage, ring hydrogenation, decarbonylation and other carbon-loss pathways can support the design of catalysts that improve deoxygenation efficiency and product stability without excessive hydrogen consumption or carbon loss. For biomass gasification, DFT-derived networks for CH_4 reforming, carbon removal and WGS/RWGS can be coupled with microkinetic and process simulations to regulate H_2/CO ratios and match syngas composition to downstream hydrogen production and methanol synthesis. DFT should therefore not be regarded as a stand-alone source of plant operating parameters. Future studies should establish a closed validation loop linking DFT descriptors, kinetic models, reactor-scale simulations and pilot-scale measurements, so that molecular calculations provide quantitative constraints for catalyst selection, process-window optimisation and scale-up rather than isolated explanations of individual elementary steps.

7. Conclusion

This review shows that DFT has become an essential tool for interpreting biomass thermochemical conversion, but its strongest role is mechanistic discrimination rather than direct product prediction. In primary pyrolysis, DFT helps identify bond-cleavage, dehydration, ring-opening and repolymerization routes. In tar removal, bio-oil upgrading and syngas conditioning, it clarifies adsorption, deoxygenation, reforming, oxygen transfer and carbon-removal steps on catalytic surfaces.

The reliability of these conclusions depends on model representativeness. Monomers, dimers, clean surfaces and isolated adsorbates are useful controlled models, but they cannot fully describe heterogeneous biomass, multicomponent tar, complex bio-oil, ash-containing char, coke-covered catalysts or dynamic gas mixtures. No single adsorption energy, oxygen-affinity descriptor or activation barrier can predict performance across the four conversion stages. Observable selectivity and stability emerge from competing pathways, surface coverage, active-site regeneration and catalyst evolution.

Within these limits, DFT can still guide cleaner biomass valorization. Its value lies in identifying which molecular steps control tar and coke formation, carbon retention, hydrogen consumption, H_2/CO regulation and catalyst stability. The next advance will come from experimentally constrained, coverage-dependent reaction networks that connect molecular mechanisms with engineering indicators for pollution control and solid-waste resource recovery.

Author Contributions

Ying Wang: conceptualization, writing; Baofeng Zhao: supervision, editing; Chongmin Wang: investigation, analysis; Haibin Guan: methodology; Lei Chen: visualization; Bari Wulan: investigation; Laizhi Sun: analysis; Tianyi Liu: visualization; Krishnaswamy Nandakumar: methodology; Wanning Zheng: resources; Ying Bo: supervision.

Data Availability

The data supporting the findings of this study are available from the corresponding author upon reasonable request.

Conflicts of Interest

No conflict of interest exists in the submission of this manuscript, and the manuscript is approved by all authors for publication. I declare on behalf of my co-authors that the work described is original research that has not been published previously and is not under consideration for publication elsewhere, in whole or in part. All the listed authors have approved the enclosed manuscript.

Funding

This work was supported by the Deep Earth National Science and Technology Major Project-Helium Enrichment and Detection in Natural Gas Reservoirs of Oil and Gas Fields

(2025ZD1010504), Shandong Key Talent Project (2024YSYY-005), Natural Science Foundation of Shandong Province (ZR2023ME175), Jinan's 20 new universities (202228123), Jinan's 20 new universities (202333025), the Innovation Ability Improvement Project of Small and Medium-sized Science and Technology Enterprises in Shandong Province (2023TSGC0176), Shandong Provincial Technology Innovation Guidance Program (Central Government-Guided Local Science and Technology Development Fund) (YDZX2024014), and the Pilot Project of Integration of Science, Education and Industry Innovation of Qilu University of Technology (Shandong Academy of Sciences) (2022GH010), the National Natural Science Foundation of China (22302104), the Natural Science Foundation of Shandong Province (ZR2023QB234), the Innovation Ability Improvement Project of Small and Medium-sized Science and Technology Enterprises in Shandong Province (2024TSGC0129 and 2024TSGC0024).

References

[1] Alonso DM, Bond JQ, Dumesic JA. Catalytic conversion of biomass to biofuels. *Green Chemistry*. 2010, 12 (9): 1493-1513. [Google Scholar] [CrossRef]

[2] Huber GW, Iborra S, Corma A.. Synthesis of Transportation Fuels from Biomass: Chemistry, Catalysts, and Engineering. *Chemical Reviews*. 2006, 106 (9): 4044–4098. [Google Scholar] [CrossRef]

[3] Lin L, Han X, Han B, *et al*. Emerging heterogeneous catalysts for biomass conversion: studies of the reaction mechanism. *Chemical Society Reviews*. 2021, 50 (20): 11270–11292. [Google Scholar] [CrossRef]

[4] Bridgwater AV. Review of fast pyrolysis of biomass and product upgrading. *Biomass and Bioenergy*. 2012, 38: 68–94. [Google Scholar] [CrossRef]

[5] Shen Y, Fu Y. Advances in in *situ* and *ex situ* tar reforming with biochar catalysts for clean energy production. *Sustainable Energy & Fuels*. 2018, 2 (2): 326–344. [Google Scholar] [CrossRef]

[6] Mortensen PM, Grunwaldt JD, Jensen PA, *et al*. A review of catalytic upgrading of bio-oil to engine fuels. *Applied Catalysis A: General*. 2011, 407: 1–19. [Google Scholar] [CrossRef]

[7] Wang Q, Song H, Pan S, *et al*. Initial pyrolysis mechanism and product formation of cellulose: An Experimental and Density functional theory (DFT) study. *Scientific Reports*. 2020, 10: 1-18. [Google Scholar] [CrossRef]

[8] Shen Q, Fu Z, Li R, *et al*. A study on the pyrolysis mechanism of a β-O-4 lignin dimer model compound using DFT combined with Py-GC/MS. *Journal of Thermal Analysis and Calorimetry*. 2020, 146 (4): 1751–1761. [Google Scholar] [CrossRef]

[9] Nørskov JK, Abild-Pedersen F, Studt F, *et al*. Density functional theory in surface chemistry and catalysis. *Proceedings of the National Academy of Sciences*. 2011, 108 (3): 937–943. [Google Scholar] [CrossRef]

[10] Zhang J, Huang X. A critical review of unraveling lignin pyrolysis mechanisms by computational chemistry: ReaxFF MD and DFT. *Journal of Analytical and Applied Pyrolysis*. 2026, 193: 1-25. [Google Scholar] [CrossRef]

[11] Wang S, Guo X, Liang T, *et al*. Mechanism research on cellulose pyrolysis by Py-GC/MS and subsequent density functional theory studies. *Bioresour Technol*. 2012, 104: 722–728. [Google Scholar] [CrossRef]

[12] Hu B, Lu Q, Jiang X, *et al*. Pyrolysis mechanism of glucose and mannose: The formation of 5-hydroxymethyl furfural and furfural. *Journal of Energy Chemistry*. 2018, 27 (2): 486–501. [Google Scholar] [CrossRef]

[13] Zhang Y, Liu C, Chen X. Unveiling the initial pyrolytic mechanisms of cellulose by DFT study. *Journal of Analytical and Applied Pyrolysis*. 2015, 113:621–629. [Google Scholar] [CrossRef]

[14] Hu B, Lu Q, Zhang Z-X, *et al*. Mechanism insight into the fast pyrolysis of xylose, xylobiose and xylan by combined theoretical and experimental approaches. *Combustion and Flame*. 2019, 206: 177–188. [Google Scholar] [CrossRef]

[15] Hu B, Zhang WM, Guo XW, *et al*. Experimental and computational study on xylan pyrolysis: The effect of branch structures. *Fuel*. 2025, 386: 1-11. [Google Scholar] [CrossRef]

[16] Dai G, Wang G, Wang K, *et al*. Mechanism study of hemicellulose pyrolysis by combining in-situ DRIFT, TGA-PIMS and theoretical calculation. *Proceedings of the Combustion Institute*. 2021, 38 (3): 4241–4249. [Google Scholar] [CrossRef]

[17] Huang J, Liu C, Wu D, *et al*. Density functional theory studies on pyrolysis mechanism of β-O-4 type lignin dimer model compound. *Journal of Analytical and Applied Pyrolysis*. 2014, 109: 98–108. [Google Scholar] [CrossRef]

[18] Elder T, Beste A. Density Functional Theory Study of the Concerted Pyrolysis Mechanism for Lignin Models. *Energy & Fuels*. 2014, 28 (8): 5229–5235. [Google Scholar] [CrossRef]

[19] Wang S, Dai G, Yang H, *et al*. Lignocellulosic biomass pyrolysis mechanism: A state-of-the-art review. *Progress in Energy and Combustion Science*. 2017, 62: 33–86. [Google Scholar] [CrossRef]

[20] Lu X, Gu X. A review on lignin pyrolysis: pyrolytic behavior, mechanism, and relevant upgrading for improving process efficiency. *Biotechnol Biofuels Bioprod*. 2022, 15 (1): 1-43. [Google Scholar] [CrossRef]

[21] Bai X, Kim KH, Brown RC, *et al*. Formation of phenolic oligomers during fast pyrolysis of lignin. *Fuel*. 2014, 128: 170–179. [Google Scholar] [CrossRef]

[22] Hosoya T, Kawamoto H, Saka S. Secondary reactions of lignin-derived primary tar components. *Journal of Analytical and Applied Pyrolysis*. 2008, 83 (1): 78–87. [Google Scholar] [CrossRef]

[23] Liu X, Sun Z, Hungwe D, *et al*. DFT insights into competitive pathways of gas evolution and char precursor formation in lignin pyrolysis. *Chemical Engineering Journal*. 2025, 526: 1-12. [Google Scholar] [CrossRef]

[24] Huang YM, Cheng YC. Adsorption and C-C bond cleavage of benzene on hematite alpha-Fe_2O_3 surfaces: a DFT mechanistic study. *Scientific Reports*. 2024, 14. [Google Scholar] [CrossRef]

[25] Trinh QT, Nguyen AV, Huynh DC, *et al*. Mechanistic insights into the catalytic elimination of tar and the promotional effect of boron on it: first-principles study using toluene as a model compound. *Catalysis Science & Technology*. 2016, 6 (15): 5871–5883. [Google Scholar] [CrossRef]

[26] Chen H, Meng J, Wang X, *et al*. Insights into the adsorption and decomposition mechanisms of tar typical model compounds (benzene, toluene and phenol) on Ni(111) surface by DFT calculations. *Journal of the Energy Institute*. 2024, 114: 1-11. [Google Scholar] [CrossRef]

[27] Wang J, Zhao B, Zhu D, *et al*. Mechanism on catalytic cracking tar with CaO-based catalysts for hydrogen-rich gas by DFT and experiments. *International Journal of Hydrogen Energy*. 2021, 46 (9): 6522–6531. [Google Scholar] [CrossRef]

[28] Chen B, Shi ZM, Jiang SJ, *et al*. Catalytic cracking mechanisms of tar model compounds. *Journal of Central South University*. 2017, 23 (1):

3100–3107. [Google Scholar] [CrossRef]
[29] Du ZY, Zhang ZH, Xu C, *et al*. Low-Temperature Steam Reforming of Toluene and Biomass Tar over Biochar-Supported Ni Nanoparticles. *ACS Sustainable Chemistry & Engineering*. 2018, 7 (3): 3111–3119. [Google Scholar] [CrossRef]
[30] Qian L, Zhao N, Guo F, *et al*. Tar microwave reforming over different biochar-based Ni catalysts by experiments and DFT. *Energy*. 2024, 304: 1-10. [Google Scholar] [CrossRef]
[31] Wang C, Zhao B, Guan H, *et al*. Magnetic field-enhanced catalytic mechanism for green syngas production from phenolic tar in biomass pyrolysis. *Energy*. 2026, 347: 1-12. [Google Scholar] [CrossRef]
[32] Wei Z, Li Y, Zhang Y, *et al*. A DFT study on catalytic cracking mechanism of tar by Ni or Fe doped CaO during biomass steam gasification. *Fuel*. 2024, 374: 1-15. [Google Scholar] [CrossRef]
[33] Lu J, Behtash S, Mamun O, *et al*. Theoretical Investigation of the Reaction Mechanism of the Guaiacol Hydrogenation over a Pt(111) Catalyst. *ACS Catalysis*. 2015, 5 (4): 2423–2435. [Google Scholar] [CrossRef]
[34] Chiara Nania MB, Laura Gueci, Francesco Ferrante, *et al*. DFT insights into competing mechanisms of guaiacol hydrodeoxygenation on a platinum cluster. *Physical Chemistry Chemical Physics*. 2023, 25 (15): 10460–10471. [Google Scholar] [CrossRef]
[35] Hensley AJR, Wang Y, Mei D, *et al*. Mechanistic Effects of Water on the Fe-Catalyzed Hydrodeoxygenation of Phenol. The Role of Brønsted Acid Sites. *ACS Catalysis*. 2018, 8 (3): 2200–2208. [Google Scholar] [CrossRef]
[36] Cheng C, Bian F, Lu C, *et al*. DFT investigation of hydrodeoxygenation of guaiacol on Fe-decorated Ni(111). *Journal of the Energy Institute*. 2024, 112: 1-9. [Google Scholar] [CrossRef]
[37] Hensley AJR, Bray J, Shangguan J, *et al*. Catalytic consequences of hydrogen addition events and solvent-adsorbate interactions during guaiacol-H_2 reactions at the H_2O-Ru(0001) interface. *Journal of Catalysis*. 2021, 395: 467–482. [Google Scholar] [CrossRef]
[38] Shangguan J, Hensley AJR, Gradiski MV, *et al*. The Role of Protons and Hydrides in the Catalytic Hydrogenolysis of Guaiacol at the Ruthenium Nanoparticle–Water Interface. *ACS Catalysis*. 2020, 10 (20): 12310–12332. [Google Scholar] [CrossRef]
[39] Wen Y, Zormpa F, Sharapa DI, *et al*. Exploring the hydrodeoxygenation of lignin β-O-4 dimer model compound and bio-oil by DFT and experimental studies. *Molecular Catalysis*. 2025, 580: 1-7. [Google Scholar] [CrossRef]
[40] Yu W, Xiong K, Ji N, *et al*. Theoretical and experimental studies of the adsorption geometry and reaction pathways of furfural over FeNi bimetallic model surfaces and supported catalysts. *Journal of Catalysis*. 2014, 317: 253–262. [Google Scholar] [CrossRef]
[41] Lin Z, Wan W, Yao S, *et al*. Cobalt-modified molybdenum carbide as a selective catalyst for hydrodeoxygenation of furfural. *Applied Catalysis B: Environmental*. 2018, 233: 160–166. [Google Scholar] [CrossRef]
[42] Jiang Z, Wan W, Lin Z, *et al*. Understanding the Role of M/Pt(111) (M = Fe, Co, Ni, Cu) Bimetallic Surfaces for Selective Hydrodeoxygenation of Furfural. *ACS Catalysis*. 2017, 7 (9): 5758–5765. [Google Scholar] [CrossRef]
[43] Xiang S, Dong L, Wang ZQ, *et al*. A unique Co@CoO catalyst for hydrogenolysis of biomass-derived 5-hydroxymethylfurfural to 2,5-dimethylfuran. *Nat Commun*. 2022, 13: 1-9. [Google Scholar] [CrossRef]
[44] Huang R, Liu C, Zhang K, *et al*. A Promising Strategy for Solvent-Regulated Selective Hydrogenation of 5-Hydroxymethylfurfural over Porous Carbon-Supported Ni-ZnO Nanoparticles. *Nanomicro Lett*. 2025, 18: 1-14. [Google Scholar] [CrossRef]
[45] Luo J, Yang W, Wang T, *et al*. Construction of Cu–Re–Ox rich interfaces for the catalytic hydrogen transfer of furfural. *Green Chemistry*. 2025, 27 (46): 14873–14882. [Google Scholar] [CrossRef]
[46] Deng Y, Pu P, Tian Z, *et al*. Transformative strategies for bimetallic catalyst screening in biomass conversion through active learning and DFT. *Applied Catalysis B: Environment and Energy*. 2025, 371: 1-12. [Google Scholar] [CrossRef]
[47] Lustemberg PG, Mao Z, Salcedo A, *et al*. Nature of the Active Sites on Ni/CeO_2 Catalysts for Methane Conversions. *ACS Catal*. 2021, 11 (16): 10604–10613. [Google Scholar] [CrossRef]
[48] Salcedo A, Lustemberg PG, Rui N, *et al*. Reaction Pathway for Coke-Free Methane Steam Reforming on a Ni/CeO_2 Catalyst: Active Sites and the Role of Metal-Support Interactions. *ACS Catal*. 2021, 11: 1-31. [Google Scholar] [CrossRef]
[49] Zou X, Zhai M, Yang D, *et al*. New insights into the mechanism of biomass char steam gasification process by oxygen-containing functional group as aromatic carbon boundaries: Experimental and DFT study. *Chemical Engineering Journal*. 2023, 465: 1-13. [Google Scholar] [CrossRef]
[50] Zhao S, Zhang Y. DFT and experimental study on the heterogeneous decomposition and steam/CO_2 reforming of gasification tar over biochar. *Fuel*. 2023, 335: 1-15. [Google Scholar] [CrossRef]
[51] Guizani C, Jeguirim M, Gadiou R, *et al*. Biomass char gasification by H_2O, CO_2 and their mixture: Evolution of chemical, textural and structural properties of the chars. *Energy*. 2016, 112: 133–145. [Google Scholar] [CrossRef]
[52] Zhang Y, Feng D, Zhao Y, *et al*. Evolution of Char Structure During In-Situ Biomass Tar Reforming: Importance of the Coupling Effect Among the Physical-Chemical Structure of Char-Based Catalysts. *Catalysts*. 2019, 9: 1-13. [Google Scholar] [CrossRef]
[53] Jiao W, Wang Z, Jiao W, *et al*. Influencing factors and reaction mechanism for catalytic CO_2 gasification of sawdust char using K-modified transition metal composite catalysts: Experimental and DFT studies. *Energy Conversion and Management*. 2020, 208: 1-11. [Google Scholar] [CrossRef]
[54] Zhao D, Wang Y, Wang G, *et al*. Exploring the mechanism of alkali metal K-catalyzed biomass char gasification using in-situ DRIFTS and molecular simulation. *Chemical Engineering Journal*. 2024, 500: 1-17. [Google Scholar] [CrossRef]
[55] Kunlun Ding AG, Alexis M. Johnson, Neil M. Schweitzer, *et al*. Stair. Identification of active sites in CO oxidation and water-gas shift over supported Pt catalysts. *Science*. 2015, 350 (6257): 189–192. [Google Scholar] [CrossRef]
[56] Li Y, Kottwitz M, Vincent JL, *et al*. Dynamic structure of active sites in ceria-supported Pt catalysts for the water gas shift reaction. *Nat Commun*. 2021, 12: 1-9. [Google Scholar] [CrossRef]
[57] Chen L, Filot IAW, Hensen EJM. Elucidation of the Reverse Water–Gas Shift Reaction Mechanism over an Isolated Ru Atom on CeO_2(111). *The Journal of Physical Chemistry C*. 2023, 127 (41): 20314–20324. [Google Scholar] [CrossRef]
[58] Wang J, Zhao B, Liu S, *et al*. Catalytic pyrolysis of biomass with Ni/Fe-CaO-based catalysts for hydrogen-rich gas: DFT and experimental study. *Energy Conversion and Management*. 2022, 254: 1-11. [Google Scholar] [CrossRef]